Three Dimensional Imaging of Translucent Objects using Volume Holographic Techniques

by

Tina Shih

Submitted to the Department of Mechanical Engineering
in Partial Fulfillment of the Requirements for the Degree of

Bachelor of Science

at the

Massachusetts Institute of Technology

June 2004

Signature of Author _____
Department of Mechanical Engineering
May 7, 2004

Certified by _____
George Barbarstathis
Esther & Harold Edgerton Assistant Professor of Mechanical Engineering
Thesis Supervisor

Accepted by _____
Ernest G. Cravalho
Professor of Mechanical Engineering
Chairman, Undergraduate Thesis Committee

Three Dimensional Imaging of Translucent Objects using Volume Holographic Techniques

by

Tina Shih

Submitted to the Department of Mechanical Engineering
On May 7, 2004 in Partial Fulfillment of the Requirements for the
Degree of Bachelor of Science Mechanical Engineering

Abstract

Plankton is a primitive form of one or several-celled organism that lives in the sea. Its behavior, its formation, and the various life patterns, when monitored, reveals a wealth of information about the sea. Three dimensional in-situ images of these semi-translucent organisms are therefore of great interest.

To better understand how volume holographic imaging works on a translucent object like plankton, this project explores the three dimensional imaging of a gummy bear. Tomographic experiments were performed both with monochromatic laser light illumination and broadband white-light illumination. It was found that unexpectedly, the white light illumination, though not a perfect tomographic setup because of the inclusion of a lot of scattered and refracted light, images better in three dimensions than the monochromatic laser illumination.

Thesis Supervisor: George Barbastathis
Title: Esther & Harold Edgerton Assistant Professor of Mechanical Engineering

Table of Contents

Page

Abstract **3**

Table of Contents **5**

Table of Figures **7**

1. Introduction **9**
1.1 Background and Purpose 9
1.2 Project Overview 9

2. Volume Holograms **10**
2.1 Applications 10
2.2 Volume Holographic Imaging 10
2.2.1 Bragg Selectivity 11
2.2.2 Point Spread Function 14

3. Tomography and Radon Transform **15**
3.1 Tomography 15
3.2 Radon Transform 15

4. Monochromatic Illumination **17**
4.1 Setup 17
4.2 Imaging Translucent Objects 17
4.3 Data 19
4.4 Discussion 24

5. Broadband Illumination **25**
5.1 Setup 25
5.2 Data 27
5.3 Discussion 33

6. Conclusions **34**

7. Future Work **34**

8. Acknowledgements **35**

9. References **35**

Table of Figures

Page

Figure 2.1 Recording a Hologram 10
Figure 2.2 Bragg Selectivity 11
Figure 2.3 Volume Holographic Imaging Setup 13
Figure 2.4 Point Spread Functions 14

Figure 3.1 Tomography 15
Figure 3.2 Projections in Radon Transform 16
Figure 3.3 2D Inverse Radon Transform 16

Figure 4.1 Monochromatic Illumination Setup 17
Figure 4.2 Tomography Tubes & PSF for Translucent Object Imaging 18
Figure 4.3 Reflective & Translucent Objects 18
Figure 4.4 Scanning in the *x*-Direction 19
Figure 4.5 Data Matrix Assembly 19
Figure 4.6 Monochromatic Data 21
Figure 4.7 Absorption data & Inverse Radon Transform 23
Figure 4.8 3D Reconstruction 23

Figure 5.1 Broadband Illumination Setup 25
Figure 5.2 Broadband Data 27
Figure 5.3 Inverse Radon Transform 29
Figure 5.4 Filtered Inverse Radon Transform 31
Figure 5.5 3D Reconstruction 33

1. Introduction

1.1 Background and Purpose

Plankton is a primitive form of one or several-celled organism that lives in the sea. Its behavior, its formation, and the various life patterns, when monitored, reveal a wealth of information about the effects of growing pollution, global warming and extensive fishing. Three dimensional in-situ images of these semi-translucent organisms require rigorous and high-resolution sampling in the time and space domains.

This type of detailed observations can be made possible using holographic cameras, first developed for this purpose by Stewart, *et al.*[1] in 1970. Although successful, these instruments were not only large and bulky, mainly resulting from the weight of the lasers and holographic films used, but they also had depth limitations. With the newer available technologies of diode lasers, digitized data and enhanced detectors since then, an autonomous real-time holographic camera can be designed and built to analyze three-dimensional volumes of seawater containing plankton with micron-scale resolution. This enhancement in capabilities would allow for the simultaneous study of entire populations of plankton in their natural habitats, creating a dynamic map of the interactions of the plankton with its immediate environment. An additional benefit to these improved holographic cameras is their potential to be lightweight and low-maintenance, critical to its value as a deep-sea instrument of data acquisition.

1.2 Project Overview

This thesis focuses on understanding how the volume hologram generates a set of data describing a three-dimensional translucent volume, and how an image of that volume can be properly reconstructed with distinguishable features and minimal noise. Before work could be performed on actual seawater samples filled with plankton, the underlying physics and methods of such data compilation is examined on a larger object. A clear gummy bear is chosen for its semblance to semi-transparent plankton, and its more functional scale. Using the principles of tomography and Radon transform, the collected data can be recombined using Matlab and other calculation intensive methods. The quality of reconstructed images resulting from two types of object illumination, broadband white-light illumination and monochromatic laser illumination, is examined in this project.

2. Volume Holograms

2.1 Background

Volume Holographic gratings were first introduced to the field of optics in the 1960s by van Heerden.[2] These diffractive elements have since then been analyzed and used widely in many areas of optical information processing. In particular, volume holograms have been widely explored as a prospect for dense and compact optical data storage media[3,4,5] to serve the growing demands of the computer industry. Other applications of volume holograms include artificial neural networks, and optical interconnects[6] and recently, as an imaging device.[7] As imaging elements, the volume hologram has been employed in various configurations, as a volume holographic telescope,[8] a confocal microscope with the volume hologram substituting for the pinhole,[9] and a scan-free three-dimensional hyperspectral imaging instrument.[10]

2.2 Volume Holographic Imaging

The idea to use holograms to capture both the amplitude and phase of light from an object as a source of 3D information about the object was first proposed by Gabor.[11] Since then, there has been a widespread use of analog and digital holograms to perform 3D and 2D imaging. While analog holography necessitates a new hologram to be recorded for each object imaged, the digital holography can be generated via a deconvolution operation for each frame the camera records.

Volume Holographic Imaging (VHI) is yet another imaging principle that can also be used for 2D and 3D imaging, but it is unlike traditional holographic imaging because of its simplicity. Any arbitrary object can be imaged onto a digital camera by a single volume hologram, which acts as a depth selective lens, obtaining 3D or 2D information in the form of an intensity map corresponding to spatial coordinates. These intensity maps can then be computationally concatenated to reconstruct an image of the object.

A hologram is created by recording the interference pattern between the reference beam and the signal beam in a photosensitive material. A volume hologram is generated through the same process, only the medium is "thicker," and the interference pattern is recorded into the entire volume.[12] Figure 2.1(a)

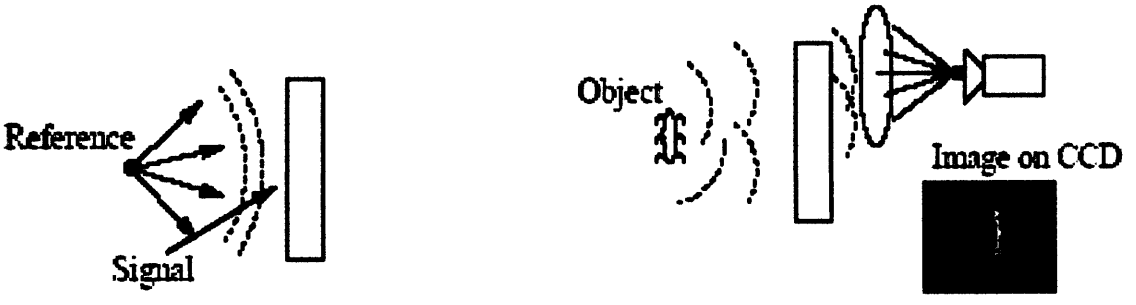

(a) (b)

Figure 2.1[13] Diagram of how volume holograms a) are recorded with the reference and signal beams and b) how they are read out with imaging optics and a detector.

For a volume holographic imaging system, the typical way to record a volume hologram is to interfere two mutually coherent beams, the point source reference beam and the plane wave signal beam, in a photosensitive material. This holographic material thickness must exceed a threshold dependent on the fringe spacing and the wavelength of the interference pattern.[14] Explained in further detail in Section 2.2.1, volume holograms are very sensitive to the nature of the illumination of the object. And only light from an object, like the example shown in Figure 2.1(a), that matches the light field during recording conditions of the volume hologram would be detected (Figure 2.1(b)). This property of volume holograms is utilized to resolve depth information for a given object to generate 2D and 3D images. All the necessary information is gathered via scanning techniques, or multiplexing holograms together to examine various parts of the object simultaneously.[10]

Volume holographic imaging systems can function under both active and passive illumination. Typical active illumination is monochromatic laser light, where the system incorporates the light that illuminates the object as part of the system. Conversely, passive illumination systems depend on ambient illumination to provide the light needed for imaging, as in broadband or white light systems. Both will be discussed in this paper, and compared for the 3D imaging of translucent objects.

2.2.1 Bragg Selectivity

A volume hologram can be used as an 3D imaging device if it can diffract in the Bragg regime. In the Bragg regime, there is one single diffracted order as opposed to the multiple diffracted orders in the Raman-Nath regime of thin holograms. This is a result of the phenomenon termed *Bragg selectivity*. This characteristic of volume holograms is then exploited as depth-selective instrument to image reflective objects.

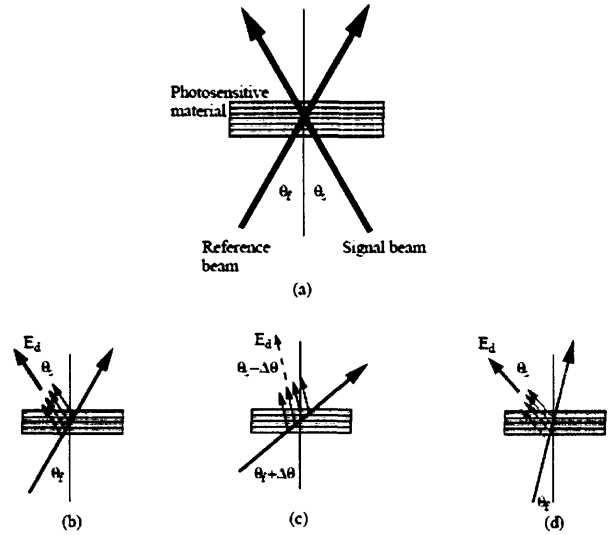

Figure 2.2[13] Bragg selectivity of volume holograms. (*a*) Recording a volume hologram. (*b*) Using a replica of the reference beam, there is a Bragg matched output. (*c*) Bragg mismatched readout results in a weak diffracted field. (*d*) A Bragg degenerate beam yields a strong diffracted beam. The Bragg degenerate beam is of a different wavelength and is incident at a different reference angle governed by Bragg selectivity.

After the recording process, the hologram is probed with light from an object. Three types of diffraction can result depending on the relationship of the probe beam to the reference beam.

1. *Bragg matched* – Figure 2.2(b), where the probe beam is an exact replica of the reference beam used to record the hologram. At the output, the full diffraction efficiency as recorded into the hologram initially can be detected.
2. *Bragg mismatched* – Figure 2.2(c), where the probe beam is not the same as the reference beam. Whether it is at a different angle of incidence or location or wavelength, the volume hologram responds to the probe beam's deviation from the reference beam by not diffracting at all.
3. *Bragg degenerate diffraction* – Figure 2.2(d) occurs when a combination of changes in the wavelength and the angle of incidence such that the diffraction is of the same magnitude as it would be were it to be Bragg matched. To reduce the amount of scanning required for the volume hologram imaging system, this particular degeneracy property is employed.[13]

The diffracted field at the detector plane consists of the substitution of many different expressions, including the paraxial approximation for the reference beam

$$E_f(\mathbf{r}) = \exp\left\{i2\pi\frac{z-z_f}{\lambda} + i\pi\frac{(x-x_f)^2+(y-y_f)^2}{\lambda(z-z_f)}\right\}. \qquad (1)$$

where the term $1/\lambda(z-z_f)$ is not accounted for because it varies much slower with z than the exponential term. This equation is combined with the signal beam in the paraxial approximation, expressed as

$$E_s(\mathbf{r}) = \exp\left\{i2\pi\left(1-\frac{\theta_s^2}{2}\right)\frac{z}{\lambda} + i2\pi\theta_s\frac{x}{\lambda}\right\}. \qquad (2)$$

The recording of these two beams can be characterized by the index modulation now in the hologram as

$$\Delta\epsilon(\mathbf{r}) \propto E_f^*(\mathbf{r})E_s(\mathbf{r}). \qquad (3)$$

where E_f^* is the complex conjugate of E_f. Only one of four resulting product terms survives in providing significant Bragg diffraction, as the rest are all Bragg mismatched.

Assuming that a probe field $E_p(\mathbf{r})$ illuminates the hologram, and knowing the index of refraction modulation of the volume hologram from Eq. 3, the response of the volume hologram to $E_p(\mathbf{r})$ can be calculated by

$$E_d(\mathbf{r}'') = \sqrt{\eta}\int E_p(\mathbf{r})\,\Delta\epsilon(\mathbf{r})\,G(\mathbf{r}''-\mathbf{r})\,d^3\mathbf{r}. \qquad (4)$$

For an object at the location of the probing point source defined by x_p, y_p, z_p, the paraxial approximation, the spatial beam that emanates from the hologram is

$$E_p(\mathbf{r}) = \exp\left\{i2\pi\frac{z-z_p}{\lambda} + i\pi\frac{(x-x_p)^2+(y-y_p)^2}{\lambda(z-z_p)}\right\}. \qquad (5)$$

Consequently, a combination of Eq. 1-5 finds the diffracted field at the detector plane to be

$$E_d(x', y') = 2\pi R^2 \sqrt{\eta} \int_{-L/2}^{L/2} \exp\{i\pi C(z)\}\, \mathcal{L}\,(2\pi A(z) R^2, 2\pi B(z) R)\, dz. \tag{6}$$

where the coefficients are

$$A(z) = \frac{1}{\lambda(z - z_f)} - \frac{1}{\lambda(z - z_p)}; \tag{7}$$

$$B_x(z) = -\frac{x_p}{\lambda(z - z_p)} + \frac{x_f}{\lambda(z - z_f)} - \frac{x'}{\lambda F} + \frac{\theta_s}{\lambda}; \tag{8}$$

$$B_y(z) = -\frac{y_p}{\lambda(z - z_p)} + \frac{y_f}{\lambda(z - z_f)} - \frac{y'}{\lambda F}; \tag{9}$$

$$B(z) = \sqrt{B_x(z)^2 + B_y(z)^2}; \tag{10}$$

$$C(z) = \frac{x_p^2 + y_p^2}{\lambda(z - z_p)} - \frac{x_f^2 + y_f^2}{\lambda(z - z_f)} + \left(\frac{x'^2 + y'^2}{\lambda F^2} - \frac{\theta_s^2}{\lambda}\right) z. \tag{11}$$

Figure 2.3 depicts the typical setup for such data acquisition. If light scattered from the object has a component that is Bragg matched to the hologram, some diffraction is generated, and can therefore be detected. Parts of the object that are Bragg mismatched, on the other hand, are "invisible" to the volume holographic imaging system. Monitoring the entire diffracted field, both when it "sees" the object and also when it does not, optical slicing can be performed, using the Bragg selectivity as a depth-sensitive component, similar to a confocal microscope.

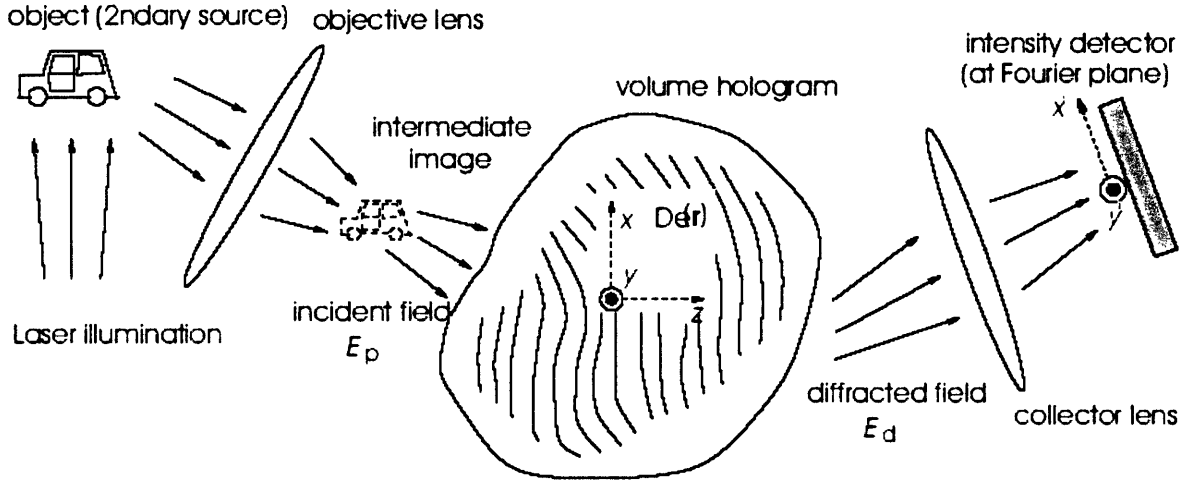

Figure 2.3[13] Diagram showing an active Volume Holographic Imaging system. The diffracted beam is monitored by a CCD intensity detector to see whether or not the light contains any Bragg matched and/or degenerate components.

2.2.2 Point Spread Function

The point spread function (PSF) determines the resolution of the imaging system. Thus, the PSF determines the quality of the images obtained from a given geometry of a volume holographic imaging system. The PSF is the intensity response of the volume holographic imaging system to any deviation of the input source location from the hologram's reference location, inherently determined in the hologram when it is recorded.

The Point Spread Function can be obtained from the total diffracted field intensity

$$\left|E_d(x', y'; x_p, y_p, z_p)\right|^2.$$

which is a function of the location of observation at the detector plane, where x' and y' are camera coordinates and the location of the probing point source, indicated by x_p, y_p, z_p.

From the Bragg selectivity of the hologram, the *degeneracy* circle helps determine how the resolution would change as a function of displacement, and can be calculated as follows

$$\Delta r' = \frac{2\lambda F}{L\theta_s}.$$

where L is the thickness of the hologram, θs is the angle of the signal beam, and F is the focal length of the lens used in the system.

To obtain a PSF of the system, the intensity at the detection plane of the volume holographic imaging system is measured as the probe is displaced. This was measured both for lateral (x-axis) and longitudinal (z-axis) to find out indicate roughly how far two distinct objects can be separated in that axial direction and still be resolved and imaged by the system (Figure 2.4(a,b)). For comparative purposes, the full width half maximum (FWHM) of the PSF is used to gauge resolution capacities. It follows that the narrower the PSF observed, the better the imaging system would perform, simply because the narrower width makes the system more selective in terms of what input light it would admit to generate a Bragg matched condition. Even though this particular definition of the PSF neglects the noise found in the volume holographic imaging system, it can be used as a good unit of comparison between this and other imaging systems.

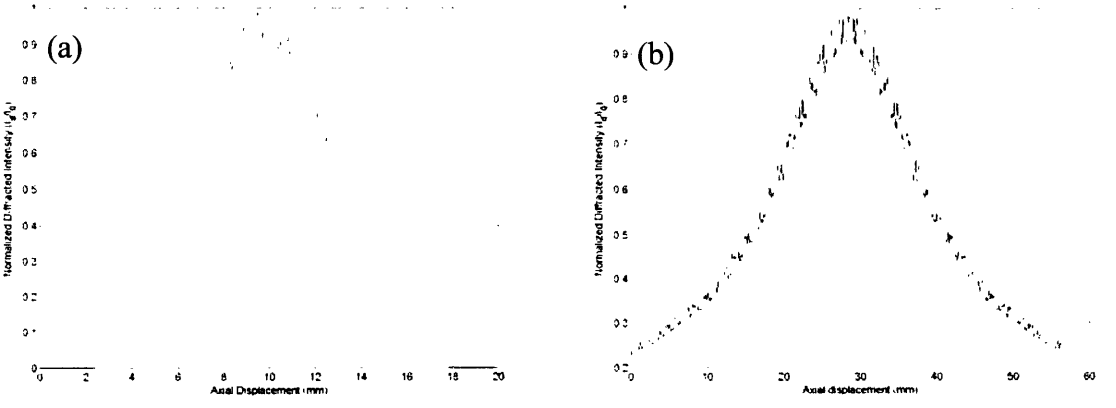

Figure 2.4 (a) Lateral point spread function for hologram and setup as described in Section 4. (b) Longitudinal point spread function of the same setup.

3. Tomography and Radon Transform

3.1 Tomography

Tomography is a non-invasive imaging technique where the image of an object are reconstructed from projections. Much like magnetic resonance imaging (MRI),[15] X-ray computerized tomography (CT) and positron emission tomography (PET) and many other tomographic techniques, there is a class of 3D tomographic imaging systems. Through this process, the information about the object is collected as projections, much like the shadow depicted in the X-Ray computerized tomography example shown in Figure 3.1. In CT, the Radon transform of the linear attenuation map can be yielded from the negative logarithm of the value of the incident photon counts divided by the measured photon counts. Radon transform inversion then convert the information back to original object coordinates, thus creating an image. The same idea can be applied to tomographic imaging using volume holograms and intensity maps. Most of these tomographic imaging systems require the object to be scanned in at least one dimension to derive all the necessary information for reconstruction.

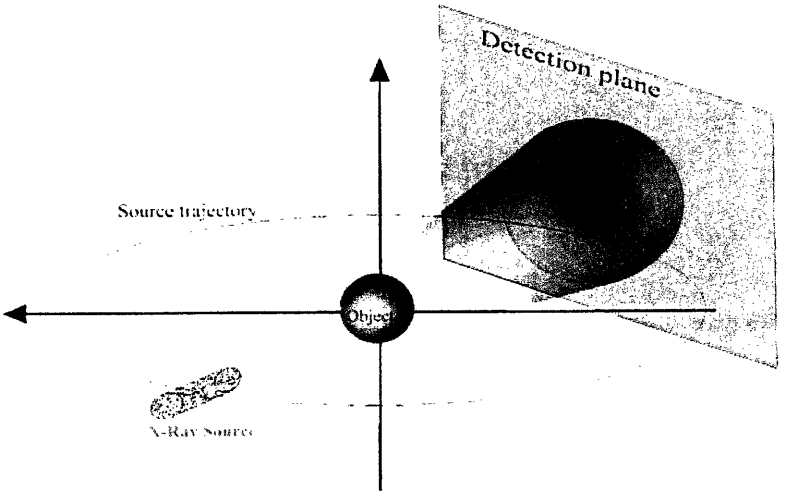

Figure 3.1 This figure shows the idea of tomography as applied to X-Ray computerized tomography.[16] Tomographic imaging using volume holograms relies on the same idea of gathering a series of projections from an object to determine its geometry.

3.2 Radon Transform

The Radon transform can be defined by [17,18,19]

$$\begin{aligned} R[p,\tau][f(x,y)] &= \int_{\infty} f(x,\tau - px)\,dx \\ &= \int_{-\infty}^{\infty}\int_{-\infty}^{\infty} f(x,y)\delta[y - (\tau - px)]\,dy\,dx \\ &\equiv U(p,\tau). \end{aligned}$$

where p is the slope of a line and τ is its intercept. The inverse Radon transform is

$$f(x,y) = \frac{1}{2\pi}\int_{-\infty}^{\infty} \frac{d}{dy} H[U(p, y - px)]\, dp.$$

where H is a Hilbert transform. The transform can also be defined by

$$R^{l}(r,\alpha)[f(x,y)] = \int_{-\infty}^{\infty}\int_{-\infty}^{\infty} f(x,y)\,\delta(r - x\cos\alpha - y\sin\alpha)\, dx\, dy.$$

where r is the perpendicular distance from a line to the origin and α is the angle formed by the distance vector.

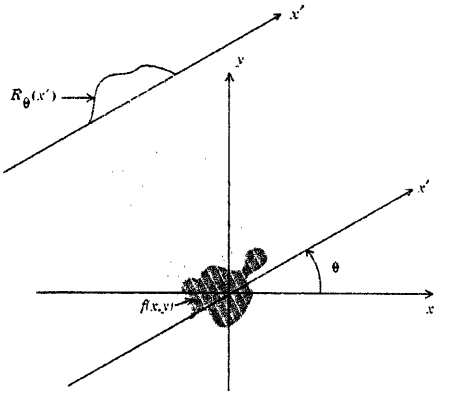

Figure 3.2 Shows an example of the parameters in Radon transform, where *f(x,y)* denotes the brightness of the image and $R_\theta(x')$ is the projection at angle theta.

Matlab has a demo function of the Radon transform and the inverse transform in 2D. The theory can be easily extrapolated for 3D objects and images. One can see that an increase in the number of views in the θ direction would generate an enhancement in the quality of the reconstruction.

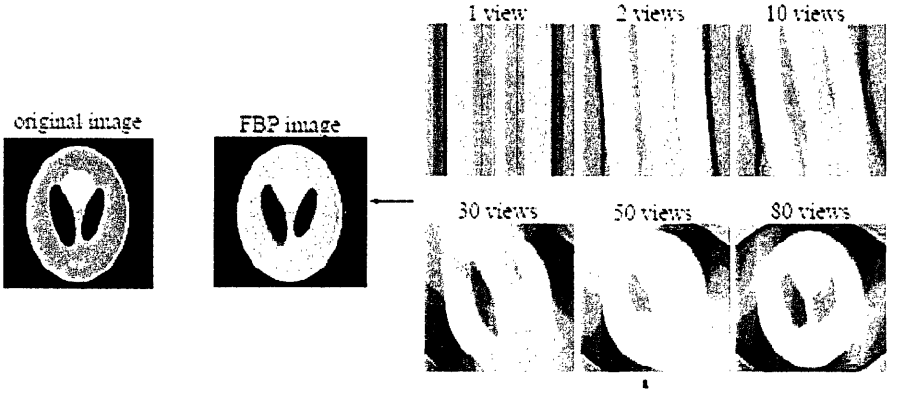

Figure 3.3 Matlab example of the 2D Shepp-Logan Phantom being reconstructed by Radon Transform computing.

4. Monochromatic Illumination

4.1 Setup

A doubled Nd:Yag CW laser (λ = 532 nm) was used for both recording and imaging in this experiment. Figure 4.1 shows the light from the laser focused through an objective and collimated to become a plane wave. A cylindrical lens then focuses the light down to a vertical line with which the bear is scanned in three dimensions, x, y, and θ. Two dimensional scanning was performed using two orthogonal Newport CMA-25CCCL actuators and a rotational actuator. The collection optics included focusing lenses to direct the light from the object to the volume hologram and then from there into a Jai CV235 industrial CCD camera.

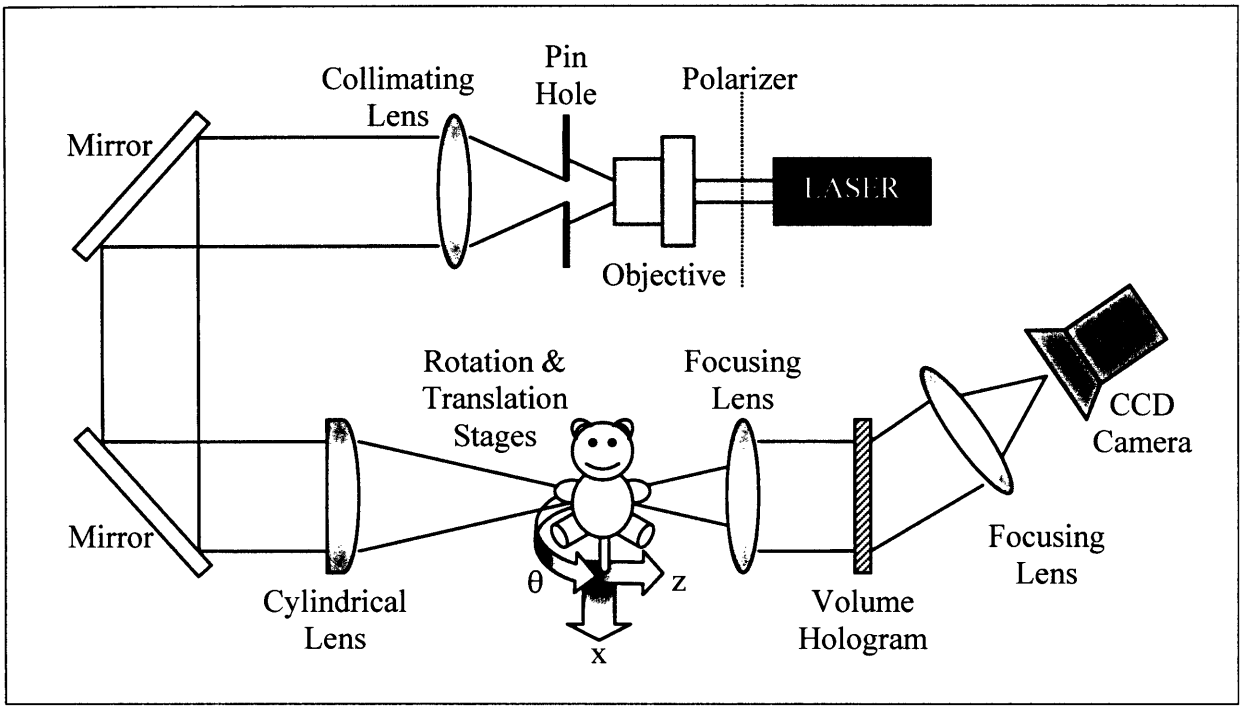

Figure 4.1 Setup of the Gummy Bear in the Monochromatic Laser Illumination scheme.

4.2 Imaging Translucent Objects

The volume holographic imaging theory presented in Section 2 applies in the same way to all objects, whether reflective or translucent. The distinction is that for reflective objects, the volume hologram collects information from a surface (Figure 4.2(a)), whereas for translucent object, the volume hologram collects information from the entire volume of the object (Figure 4.2(b)). A translucent object not only reflects light from its front surface, but it also transmits a certain portion of light through; some of that light is scattered, some of it diffracted, some of it reflected and some refracted. For the case of imaging the gummy bear with monochromatic illumination, the input light source is coherent, which, according to Huygens' Principle, each point is a point source in this translucent volume. But when each of these point sources are summed up, the interference generated as a result is the hardest source of noise to overcome in

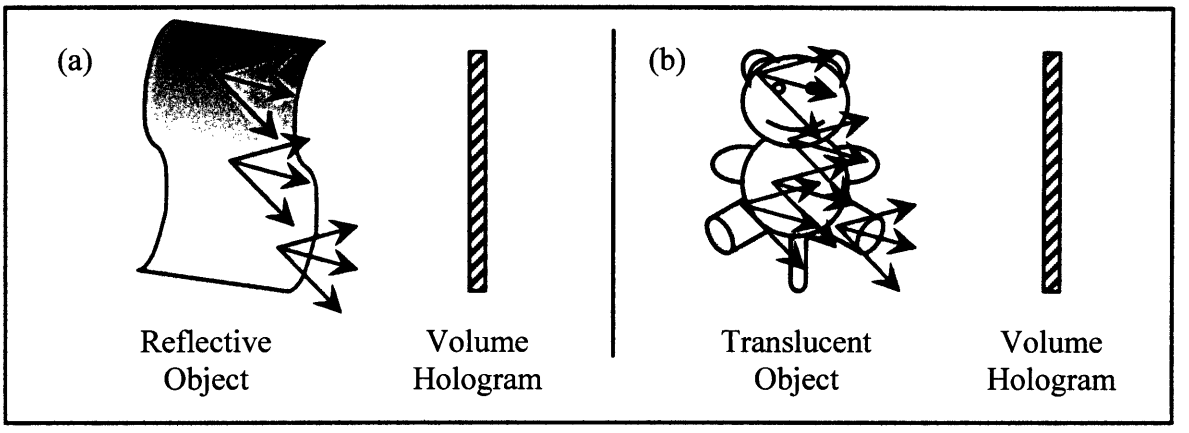

Figure 4.2 (a) Point source collection by a volume hologram off a surface of a reflective object. (b) Point source collection by a volume hologram off the entire volume of a reflective object with much more interference detected by the system.

imaging. The scatter is exacerbated by the non-uniform sugary substance of the gummy bear, which has random air bubbles inclusions. The only way around this problem is to reduce the analysis of the object into "tubes" of light (Figure 4.3(a)), and in scanning, monitor the light modulations in each tube, which, when combined would reveal the object geometry. In order to simulate these tubes of light, the selectivity in the axial (longitudinal or z) direction must be expanded to incorporate the gummy bear (Figure 4.3(b)).

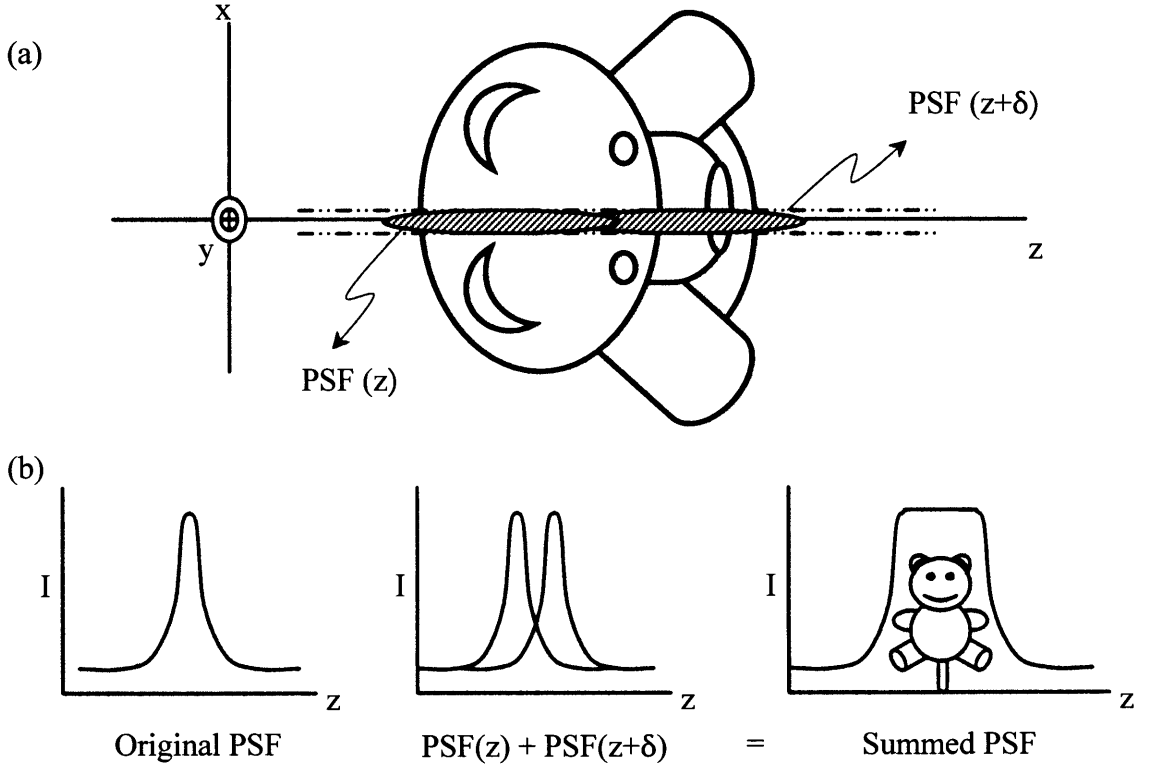

Figure 4.3 (a) Creating a "tube" of light scanning in the z-direction with multiple PSFs. (b) Concatenating PSFs to include the whole of the bear.

4.3 Data

Data from the camera are collected from the setup as described in Figure 4.1, then stitched together. The data from the scanning in the two z locations (Figure 4.3(a)) are collected then summed, and the data from the scanning range as described in Figure 4.4 in the x direction are compressed (Figure 4.5(a)) and concatenated (Figure 4.5(b)), forming an image for each angle (Figure 4.5(c)). The actual data that has been compiled for each angular rotation of the gummy bear is seen in Figures 4.6(a-f)). Once information from a 180° scan is complete, the inverse Radon transform is computed to give horizontal cross-sectional images of the bear. To look at absorption of the light by the bear, the intensity profile gathered is flipped, as seen in Figure 4.7(a). The inverse Radon transform is performed on this set of data, and outputs a cross section of the bear, and example of which is shown in Figure 4.7(b). These snapshots of the gummy bear cross sections are then pieced together to form the entire bear (Figure 4.8).

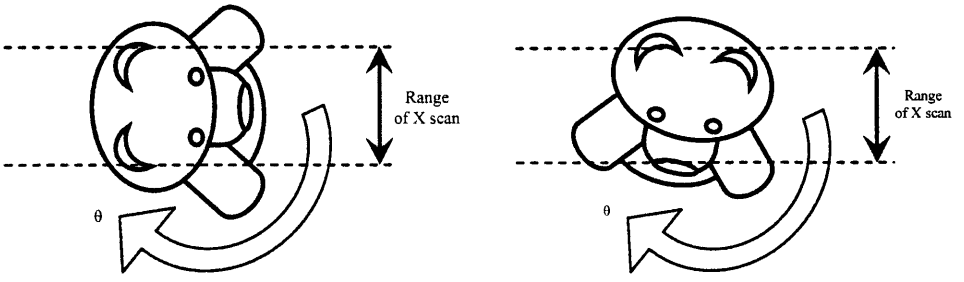

Figure 4.4 Range of x-directional scan shown with the gummy bear at various angles.

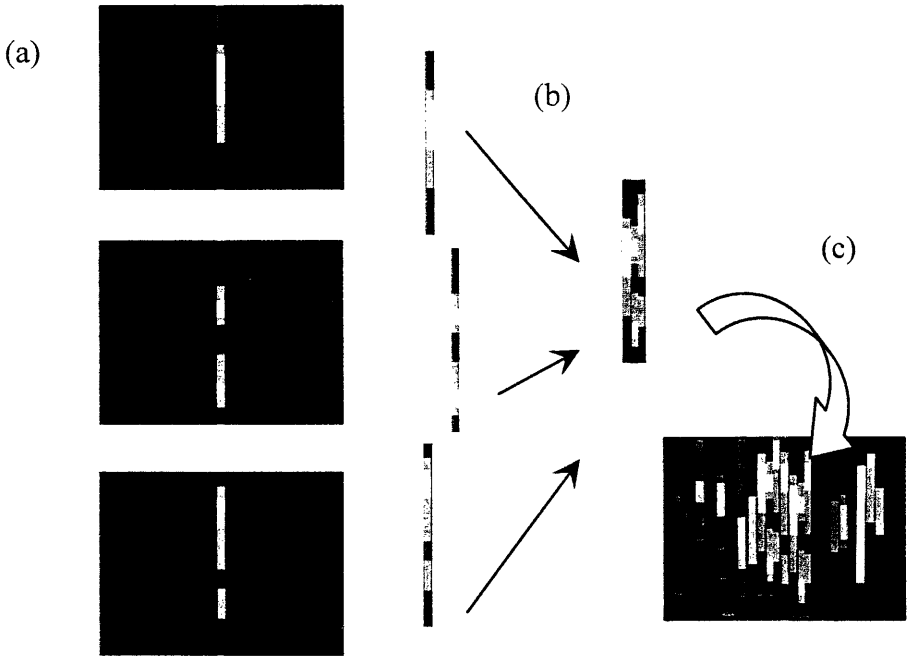

Figure 4.5 Matrix assembly process for collected data. (a) Image taken by CCD camera as it is scanned in the x direction. (b) Horizontal compression and concatenation. (c) Final image from compiled scans.

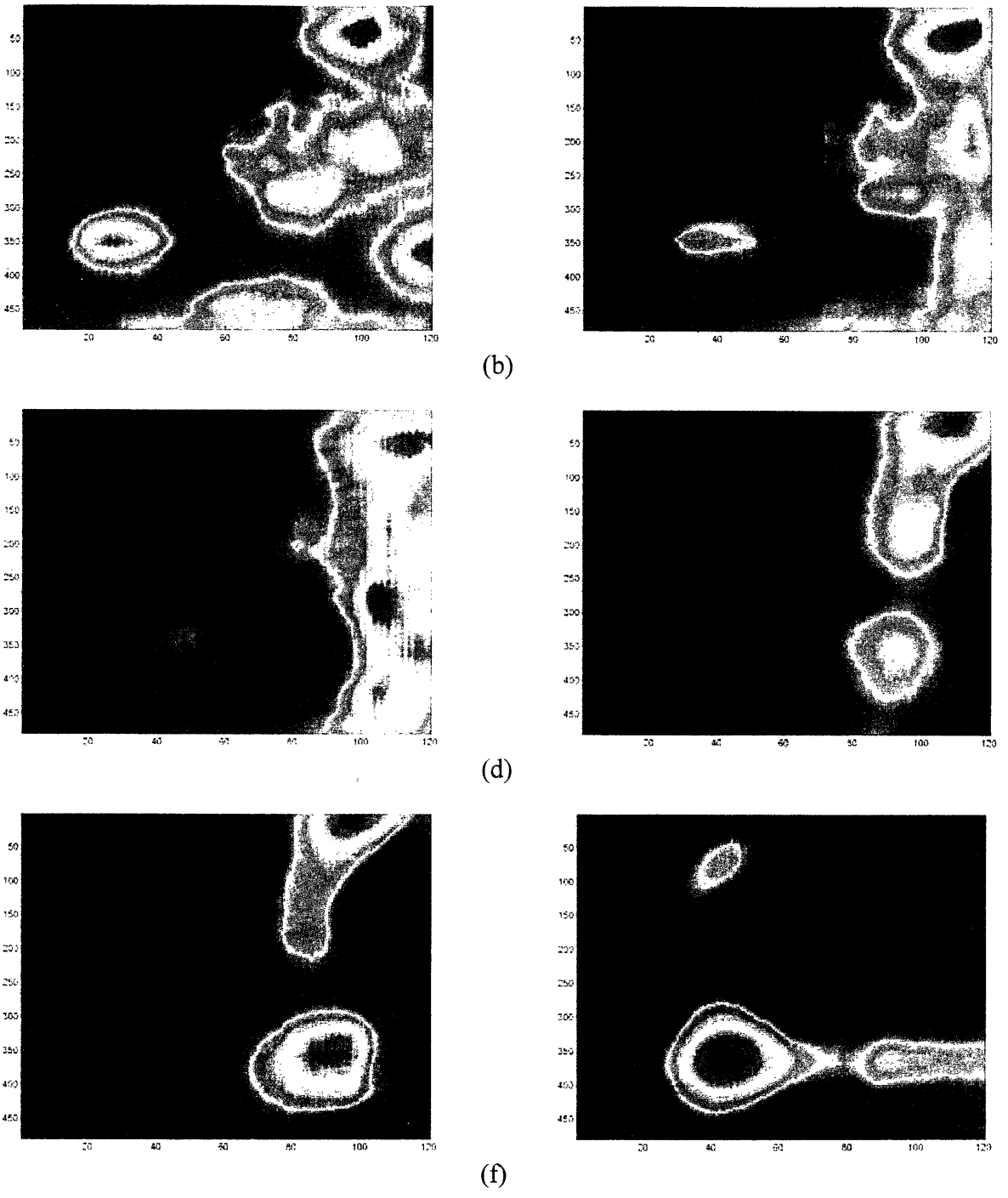

Figure 4.6 Showing scans of angles relative to the start angle. (a) 2 degrees – parts of the head and arms can be seen. (b) 13 degrees – head and arms disappear slightly. (c) 20 degrees. (d) 40 degrees. (e) 50 degrees. (f) 80 degrees.

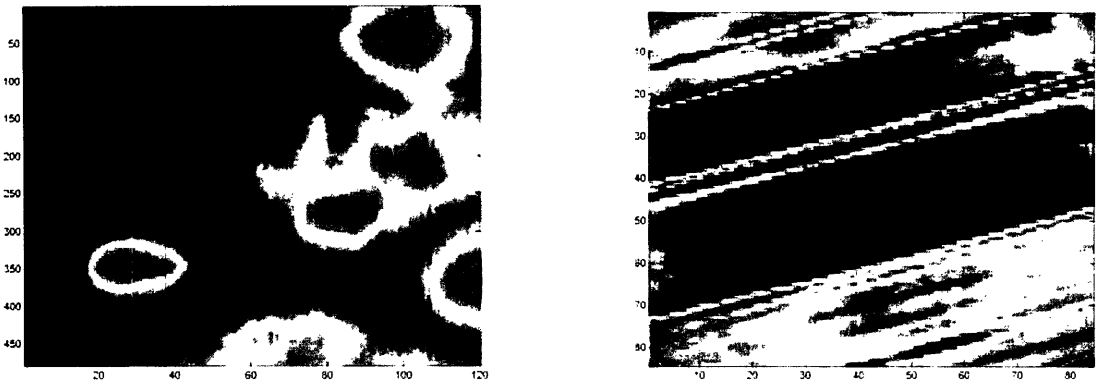

(a) (b)

Figure 4.7 Inverted scans of the bear to show its absorption. (b) the inverse Radon transformation showing the cross section of the bear.

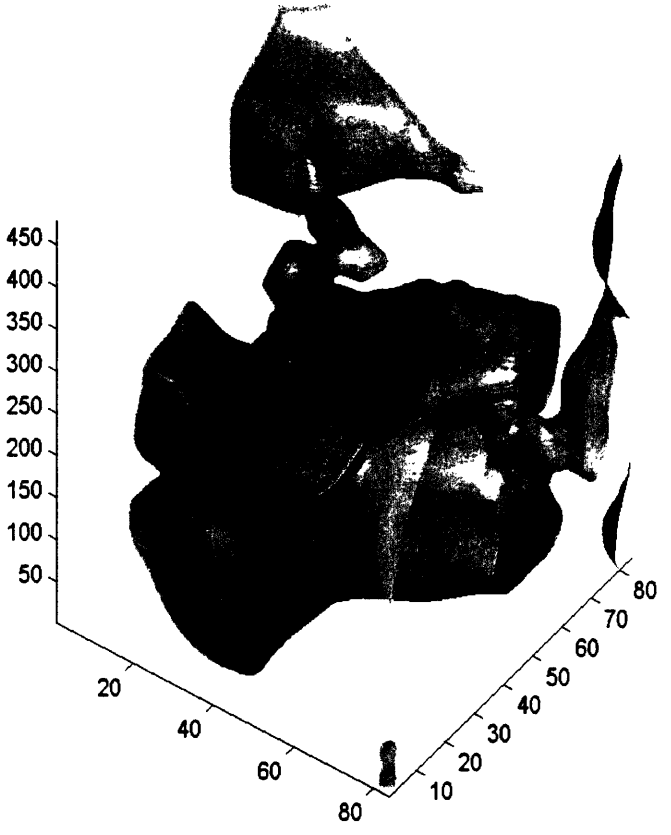

Figure 4.8 Three dimensional reconstruction from the concatenated data from all the various scans made with the monochromatic laser illumination on the bear.

4.4 Discussion

The data show that it is possible to reconstruct some form from the translucent gummy bear from these scans. The most significant reason the data did not generate a very accurate image of the gummy bear is that the input illumination is coherent. Rather than being beneficial as would have been expected from its narrower bandwidth as compared to white light, the coherent light produces far more interference inside the translucent volume, which makes the gummy bear hard to distinguish from interference noise, and therefore hard to image. This type of noise could potentially be reduced by introducing incoherent illumination into the system, whereby the interference generated would be less significant. Such incoherent illumination could be found either in broadband (white light) illumination, or even from a rainbow illumination, produced by white light reflected by a grating.

Telltale signs of improper reconstruction resulting from monochromatic laser illumination of the gummy bear can be seen from the unclear concatenated images as seen in Figures 4.5(a-f). Additionally, one can see from the inverse Radon transform that was processed from these images (Figure 4.6(b)) that there was not sufficient data to make a recognizable three dimensional reconstruction of the bear.

Another problem might result from the fact that the actuators are not perfect, and have slight, but noticeable walk-off distances, which accumulate over time. This makes the image shift, a condition that is not ideal for Radon transform calculations. The data would need to be more carefully taken with an alternate method of measuring the true distance rather than a relative distance, for example, with an interferometer or something on that level of accuracy.

One other major concern about this method is the time it requires to acquire the images for each angle. Even though the plankton holographic camera would ultimately be designed with an array of cameras to collect data from all angles simultaneously, for the current project, scanning time is the most consuming factor of data processing. Much faster electronics and mechanisms are required to speed up the process to the point where this can be made to be real-time.

5. Broadband Illumination

5.1 Setup

Broadband illumination of an object is advantageous in a volume holographic imaging setup because it eliminates the necessity to scan. The various colors are mapped to a certain location on the CCD Camera. Since each color light would pass through the material differently and also get diffracted differently by the hologram, only rotational scanning is necessary.

The laser is initially used to align the optics such that the Bragg matched diffraction from the volume hologram would be focused by the second focusing lens and into the Jai CV235 industrial CCD Camera. The laser light is then blocked and broadband illumination from a optical fiber bundle of a CUDA 250 Watt Quartz Halogen Lamp. The optical fiber is positioned such that direct light does not enter the focusing lens, but mostly through the bear, thus providing information about its three-dimensional structure.

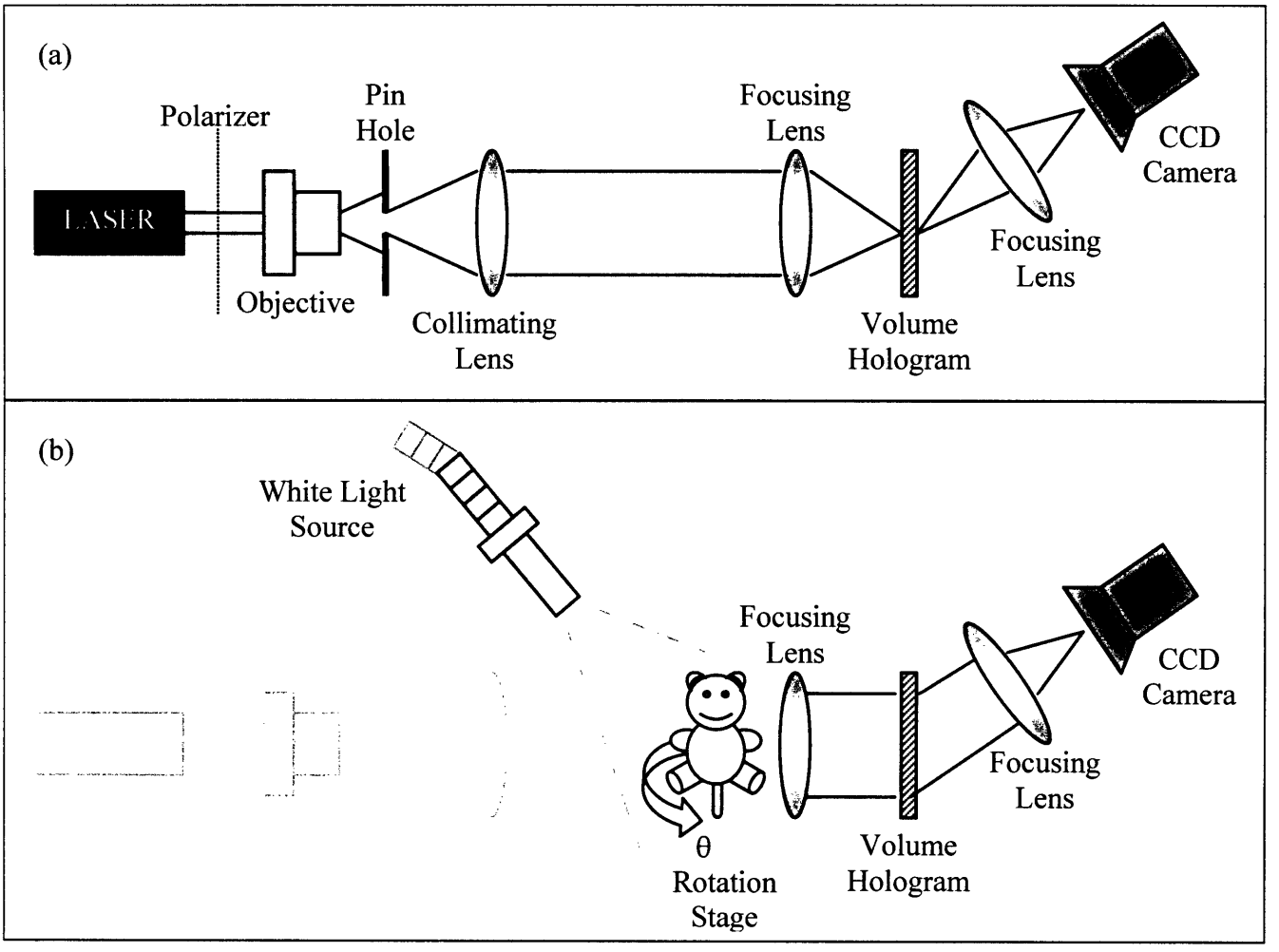

Figure 5.1 Setup of the optics and the gummy bear in the Broadband White-light Illumination scheme. (a) Setup used to align the volume hologram to the data collection optics. (b) Setup introducing the white light during data collection.

5.2 Data

Figure 5.2 shows an example of one set of measurements in the form of images taken by the CCD camera at particular angles as the gummy bear is scanned along its rotational axis.

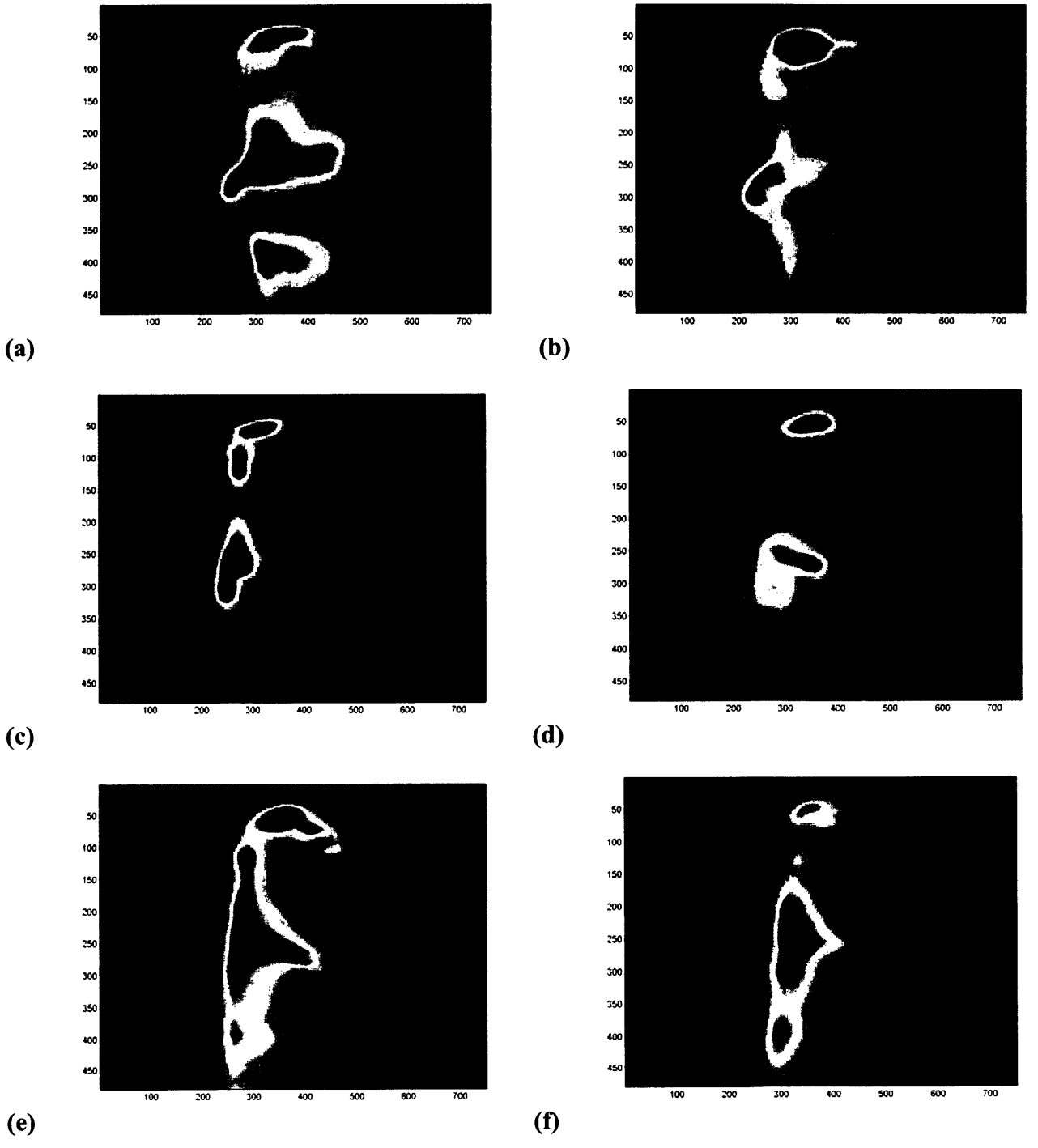

Figure 5.2 CCD Camera image taken at a variety of angles relative to the start angle. (a) 105 degrees. (b) 146 degrees. (c) 188 degrees. (d) 213 degrees. (e) 235 degrees. (f) 261 degrees.

From the data of the gummy bear image at each angle, the information is directly inverse Radon transformed, and horizontal cross sections of the bear is obtained (Figure 5.3).

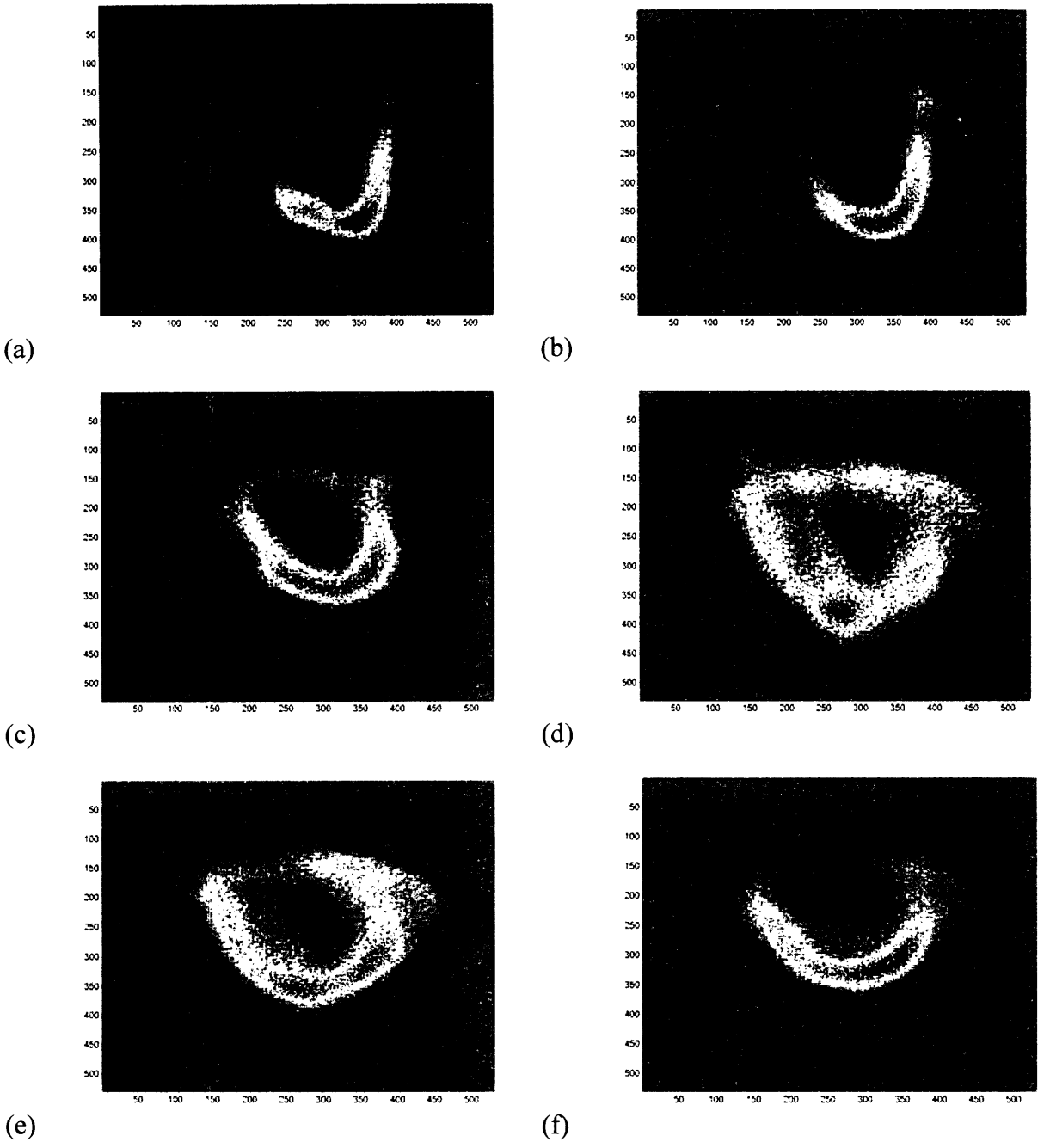

Figure 5.3 Horizontal cross-sections of the gummy bear generated with inverse Radon transforms. (a) 100th slice from the top – head and flanges of ears. (b) 120th slice – more head and ears. (c) 200th slice – thinner neck of the bear. (d) 340th slice – beginnings of arms and shoulders sprouting. (e) 360th slice – more arms. (f) 400th slice – smooth round tummy section.

Because the information gathered in this method contains a lot of noise, a Hann filter was applied to the Radon inverse transform function such that it eliminated much of the background noise, yielding better results, as can be seen in Figure 5.4 (a-f) for the same set of angles presented in Figure 5.3 (a-f).

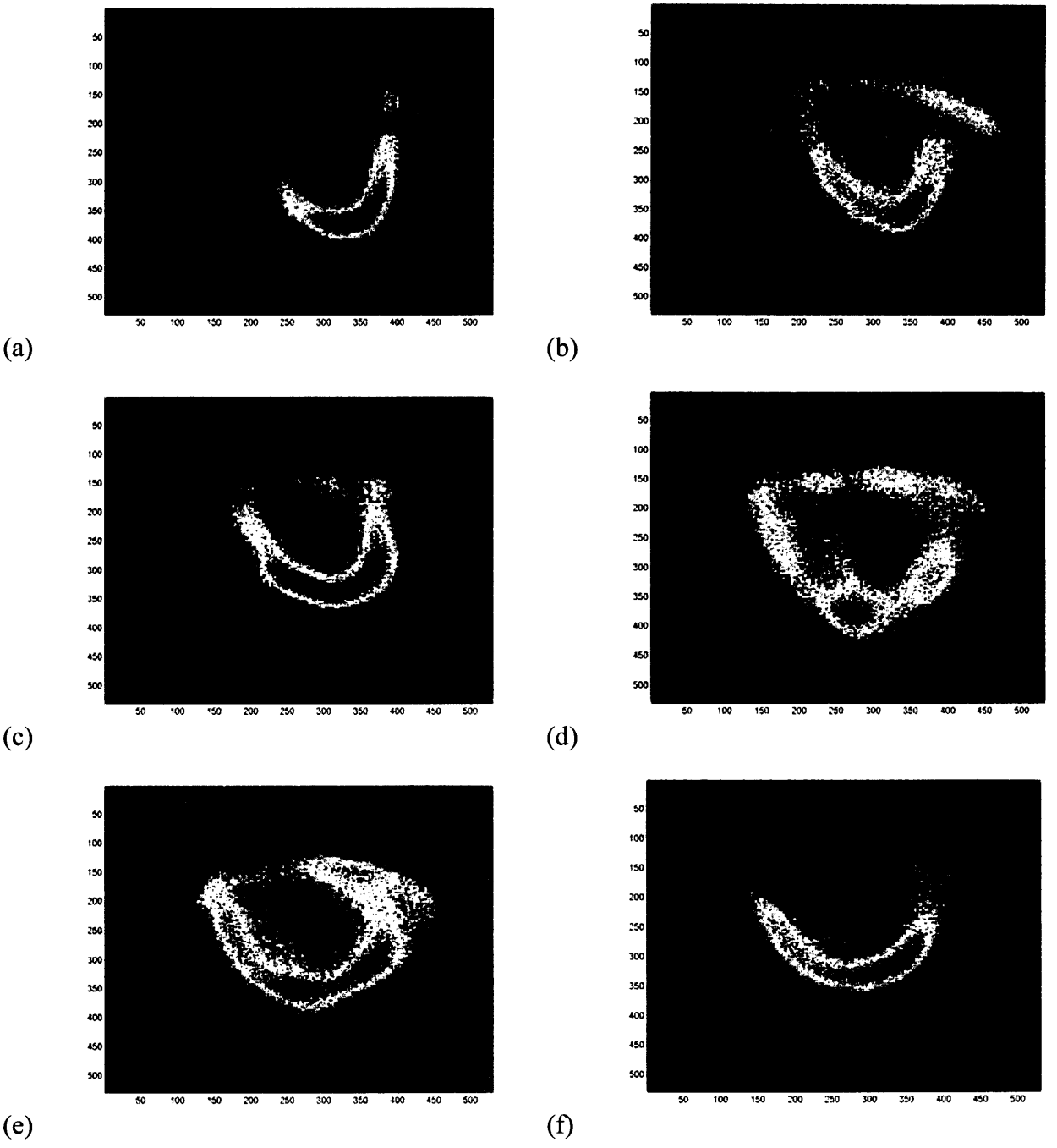

Figure 5.4 Horizontal cross-sections of the gummy bear generated with Hann filtered inverse Radon transforms. (a) 100th slice from the top – head and flanges of ears. (b) 120th slice – more head and ears. (c) 200th slice – thinner neck of the bear. (d) 340th slice – beginnings of arms and shoulders sprouting. (e) 360th slice – more arms. (f) 400th slice – smooth round tummy section.

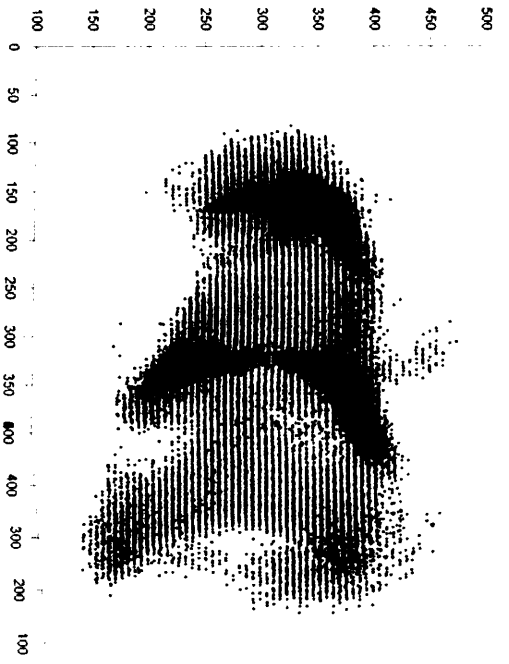

Figure 5.5 Three Dimensional Reconstruction of the bear using only x,y,z coordinates of points that are found to be orange or red (higher intensity) in the horizontal cross-sectional slices produced by Hann filtered inverse Radon transformation.

5.3 Discussion

As mentioned in Section 2.2.1, Bragg degenerate diffraction occurs when there is a specific value of combined shift both in the wavelength and the displacement. This color degeneracy of the volume hologram is exploited in the case of broadband illumination such that a white light plane wave is used to do line scanning, and the field of view could be expanded such that imaging speed is increased, and scanning in the x and z directions are eliminated. While there is a reduction in the amount of scanning needed, the drawback to this method is that the point spread function is much wider, and very blurred because the existence of more than one color that could be Bragg matched at one given place. Moreover, the CCD camera is a black and white intensity camera, and is therefore only sensitive to changes in intensity and not color.

The images obtained were indeed able to give fairly good snapshots of the horizontal cross sections of the bear. It can be seen that the first set of data (Figure5.2(a-f)) is definitely of a much poorer quality than then Hann filtered data (Figure 5.3(a-f)). It is particularly in this latter set of data that one could see the beginnings of the ears in Figure 5.3(a,b), and the smaller radius of the bear's neck in Figure 5.3(c), moving slowly to show signs of the two arms (Figure 5.3(d)) in the red spots and then back down through the tummy in Figures 5.3(e,f). This produces the three dimensional point cloud plotted in Figure 5.4. From the analysis, the data produced a very recognizable gummy bear. However, some detailed features were lost due to the fact that the broadband illumination no longer allows the system to distinguish between refracted, reflected, scattered, diffracted and/or direct light.

6. Conclusions

Volume holographic of a translucent object was found to be best using broadband illumination techniques. Even though a tomographic process is not perfectly utilized under broadband illumination, as can be seen from the inclusion of reflected, refracted, absorbed and scattered light in the data, the data can be interpreted to properly yield a recognizable gummy bear.

Drawbacks to the monochromatic illumination technique included the extensive scanning time, the reliability of the translation stages used, and the multiple steps involved in assembling all the data. However, the biggest disadvantage to monochromatic laser probing is that the input is coherent in nature, which generates so much interference within the three dimensional translucent object that the noise cannot be easily distinguished from the useful information. All of these artifacts contribute to the degradation of the ultimate three dimensional reconstruction of the gummy bear.

This experiment can be generalized to other applications and objects since a comparison was performed between monochromatic and broadband illumination. Broadband illumination was ultimately found to be better suited to obtain a three dimensional image of any translucent object.

7. Future Work

Future work include eliminating scanning or the scanning effects in the monochromatic illumination case. Another consideration not yet considered in this project that should be looked into further is the scaling of the imaged objects, how much detail can be resolved, and whether or not resolution could be improved. Prior to moving onto the much smaller scale on the order of plankton, an interesting set of experiments would be to see if imbedded objects in the translucent object would be able to be imaged. For example, one could look at whether or not a small grain of rice inserted into the bear be imaged properly. The final stage of these experiments is to try volume holographic imaging on plankton, first in a controlled environment, and then in situ. Hopefully, this series of better understandings will allow for a better generation of holographic cameras to be created.

8. Acknowledgements

I am grateful for the guidance of Arnab Sinha and Wenyang Sun throughout this process. A special thank you to Prof. George Barbastathis for providing me with the incentive and resources to pursue this project, in addition to his continued support and encouragement. This project was funded by the Air Force Research Laboratories (Eglin AFB) and the support of the National Science Foundation.

9. References

1 Stewart G L, Beers J R and Knox C. Application of holographic techniques to the study of marine plankton in the field and the laboratory *Proc. SPIE* 41:183–8, 1970.

2 P. J. van Heerden. Theory of optical information storage in solids. *Appl. Opt.*, 2(4):393–400, 1963.

3 E. N. Leith, A. Kozma, J. Upatnieks, J. Marks, and N. Massey. Holographic data storage in three-dimensional media. *Appl. Opt.*, 5(8):1303–1311, 1966.

4 D. Psaltis and F. Mok. Holographic memories. *Sci. Am.*, 273(5):70–76, 1995.

5 J. F. Heanue, M. C. Bashaw, and L. Hesselink. Volume holographic storage and retrieval of digital data. *Science*, 265(5173):749–752, 1994.

6 H. Lee, X.-G. Gu, and D. Psaltis. Volume holographic interconnections with maximal capacity and minimal cross talk. *J. Appl. Phys.*, 65(6):2191–2194, March 1989.

7 G. Barbastathis and D. J. Brady. Multidimensional tomographic imaging using volume holography. *Proc. IEEE*, 87(12):2098–2120, 1999.

8 A. Sinha and G. Barbastathis. Volume holographic telescope. *Opt. Lett.*, 27:1690–1692, 2002.

9 G. Barbastathis, M. Balberg, and D. J. Brady. Confocal microscopy with a volume holographic filter. *Opt. Lett.*, 24(12):811–813, 1999.

10 W. Liu, D. Psaltis, and G. Barbastathis. Real time spectral imaging in three spatial dimensions. *Opt. Lett.*, 27:854–856, 2002.

11 D. Gabor. A new microscopic principle. *Nature*, 161:777, 1948.

12 H. Coufal, D. Psaltis, and G. Sincerbox, editors. *Holographic data storage*. Springer, 2000.

13 A. Sinha, W. Sun, T. Shih and G. Barbastathis. Volume holographic imaging in transmission geometry. *Appl. Opt.*, 43(7):1533-1551, 2004

14 Pochi Yeh. Introduction to photorefractive nonlinear optics. Wiley & Sons, 1993.

15 P. Grangeat. Mathematical framework of cone beam 3D reconstruction via the first derivative of the Radon transform. In G. T. Herman, A. K. Louis, and F. Natterer, editors, *Lecture Notes in Mathematics 1497: Mathematical Methods in Tomography*. Springer-Verlag, 1991.

16 I. Trofimov. Three Dimensional X-Ray Cone-Beam Reconstruction algorithms. Institute of Automation and Electrometry SB RAS 1996-2001

17 A. G. Rann and A. I. Katsevich. *The Radon Transform and Local Tomography.* Boca Raton, FL: CRC Press, 1996.

18 A.C. Kak and M. Slaney, *Principles of Computerized Tomographic Imaging.* IEEE Press, 1988.

19 S.R. Deans. *The Radon Transform and Some of Its Applications.* New York: Wiley, 1983.